Temperature and intensity of sonoluminescence radiation in sulfuric acid

A. Moshaii,* M. A. Hoseini, S. Gharibzadeh, and A. Tavakoli-Anaraki
Department of Physics, Tarbiat Modares University, P.O. Box 14115-175, Tehran, Iran
(Received 19 March 2012; revised manuscript received 5 June 2012; published 17 July 2012)

The spectral radiation of sonoluminescence (SL) from sulfuric acid doped with various Xe concentrations has been studied in a hydrochemical simulation, including radiation effects of both continuum and line emissions. The simulation considers the same temperature for both continuum and line parts of the SL spectrum and gives results in agreement with the experiment. Also, it can properly show period-doubling dynamics for a 50 torr bubble. For most of the allowable driving pressures, it is shown that both the temperature and the intensity of SL for a 4 torr bubble are greater than those of a 50 torr bubble. However, for the range of pressures near the maximum driving conditions of the 50 torr bubble, the SL intensity of this bubble can be up to three orders of magnitude greater than the 4 torr bubble. This case, which is in agreement with the experiment, is obtained when the light-emitting region of the 50 torr bubble is about three orders of magnitude greater than the 4 torr bubble.

DOI: 10.1103/PhysRevE.86.016316 PACS number(s): 78.60.Mq, 43.35.Hl

I. INTRODUCTION

In the sonoluminescence (SL) phenomenon, energy of sound waves is concentrated inside a collapsing bubble to produce very short flashes of light [1,2]. The spectrum of a single stable sonoluminescing bubble is usually continuum and featureless, extending from 200 to 800 nm [3]. However driving the bubble by enough low pressures [4] or using nonvolatile mineral acids such as sulfuric acid [5–7] leads to appearance of molecular or atomic lines in the SL spectrum. Due to the smallness of vapor pressure of a nonvolatile acid, the energy loss by the chemical dissociation of vapor molecules at the collapse has minor effect on the adiabatic heating of the bubble. This causes a scale-up of the SL radiation from sulfuric acid up to three orders of magnitude relative to the standard SL intensity from water [8].

One of the characteristics of SL radiation from sulfuric acid is the strong dependency of the intensity on the noble gas concentration in the acid. The experiment shows that the intensity of SL from a 50 torr Xe bubble in a concentrated acid solution can be two orders of magnitude greater than the SL from a 4 torr Xe bubble in the same solution [9]. This strong difference between the bubbles of low and high noble gas concentrations proposes the question: What is the relation between the intensity and the temperature of SL from different noble gas concentrations? Also, it has not been experimentally clarified yet whether a higher SL intensity always arises from a bubble with a higher temperature. In addition, experimental approaches for determination of the SL temperature from the spectrum usually lead to two completely different temperatures from the continuum and the discrete parts of the spectrum [8]. The question of how the continuum and the discrete emissions occur during the collapse in addition to the relation between the intensity and the temperature of SL were the main motivations of the authors for a systematic study of the SL emission in this work.

The problem of simulation of the SL spectrum has been studied by many researchers [10–18]. The SL spectrum in many experiments has a good compatibility with the black body spectrum radiated from a spherical surface [19,20]. This indicates that a theoretical description of the SL emission should include the planck emission as a base of the radiation model. However, the conditions of high temperature and high pressure at the time of SL emission lead to ionization of the atoms and molecules and produce free electrons. The existence of free electrons inside the bubble can considerably disturb the planck radiation by bremsstrahlung emission from scattering of free electrons against the neutral atoms and ions. In addition, the line emission due to the excitation between bound states of the particles inside the bubble can further disturb the original planck radiation.

The simulation of SL spectrum using the basic equation of radiation transfer was first proposed by Hilgenfeldt *et al.* [10,11]. In their model, the modifications of the original Planck radiation by the effects of electron-atom and electron-ion bremsstrahlung and recombination radiation have been considered. However, they neglected the excitation of bound states, mainly because at that time, the line emission of single-bubble SL had not been observed. This model could well describe many characteristics of SL spectrum from noble gases in water. The model was successively improved and applied for various experimental data by several authors [12–15]. Especially, the modification of the model for a dense plasma leading to a reduction of the ionization potential was proposed in Ref. [13].

After the discovery of the line emission from single-bubble SL [5–8], the first simulation of the line emission in the SL spectrum was proposed by An and Li [16]. Although in Ref. [16], the refinement of the Planck emission by the effects of bremsstrahlung and recombination radiations was not considered; however, these effects were added to the model in the subsequent works [17,18]. Very recently, this model was used for description of the SL emission from different noble gases in water [18]. The radiation model we used in this work is similar to that proposed in Ref. [18]. However, we use the model for an Xe bubble in sulfuric acid to investigate the relation between the intensity and the temperature of SL in this liquid and compare the results with corresponding experimental data.

To investigate the relation between the intensity and the temperature of SL, the spectral emission from an Xe

*moshaii@modares.ac.ir

bubble in the concentrated solution of 85% sulfuric acid has been calculated in the framework of a hydrochemical model including radiation mechanisms of both continuum and line emissions. The model considers a same temperature for both continuum and line parts of the spectrum. The results indicate that for most of driving pressures, both the intensity and the temperature for a typical 4 torr bubble are greater than those of a 50 torr bubble. However, for a very narrow range of the driving pressures, in agreement with the experiment, it is possible that the SL intensity from a 50 torr bubble with a lower temperature can be considerably greater than the intensity of a 4 torr bubble with a higher temperature. In this case, the light-emitting region of the 50 torr bubble is about three orders of magnitude greater than that of the 4 torr bubble.

The success of the simulation for providing the results coherent with experiment suggests that the problem of two different temperatures for the line and the continuum emissions can possibly be resolved by fitting the experimental data with a more complete model, including both line and continuum emissions rather than using simple black body or bremsstrahlung radiation.

II. SIMULATION MODEL

The model we use to simulate the bubble evolution is a hydrochemical model considering the bubble interior as a uniform medium. The model that was successively developed by many researchers [13,21–29] can provide many characteristics of the bubble evolution and its outputs in many cases are coherent with those obtained from the solution of full Navier-Stokes equations for the bubble inside [30–32]. The uniform model includes many complexities such as heat transfer at the bubble interface [24], evaporation and condensation of both sulfuric acid and water molecules [26], chemical reactions at the collapse, and contributions of rotational and vibrational degrees of freedom in the bubble thermal energy [25,27]. In addition, different instabilities preventing the bubble from stable oscillations are considered in the model [28]. The hydrochemical model has well been described in the literature [25–29] and is not repeated here again.

By determining the bubble properties at the collapse, the SL spectrum can be calculated from a radiation model. A proper model including both continuum and discrete emission mechanisms can be developed using the radiation transfer equation for the bubble inside [33]

$$\frac{dI_\nu}{dr} = (1 - e^{-h\nu/kT_g})\kappa_\nu\left(I_\nu^{Pl} - I_\nu\right), \tag{1}$$

where I_ν is the radiation intensity with the frequency ν at the point r inside the bubble, I_ν^{Pl} is the Planck radiation at the bubble temperature T_g, and κ_ν is the absorption coefficient. The general solution of Eq. (1) for an SL bubble can be obtained from the well-known methods of the solution of a linear first-order ordinary differential equation [34]:

$$I_\nu(R) = \int_0^R \exp\left[\int_0^r \kappa'_\nu(s)ds\right]\kappa'_\nu(r)I_\nu^{Pl}(r)dr \times \exp\left[\int_0^R -\kappa'_\nu(r)dr\right], \tag{2}$$

where the quantity $\kappa'_\nu(r) = (1 - e^{-h\nu/kT_g})\kappa_\nu(r)$ is the effective absorption coefficient at the point r inside the bubble. It should be mentioned that Eq. (2) is the most general solution of Eq. (1), without any approximation. This solution is more complete than the typical solution presented in some literatures as Refs. [15,33].

Although, Eq. (2) is written versus the absorption coefficient; however, due to the presence of the factor $(1 - e^{-h\nu/kT_g})$ in the effective absorption coefficient, this equation includes all effects of both absorption and emission of radiation [33]. In addition, the equation is complete for describing all continuum and discrete radiations if their corresponding contributions are properly considered in the absorption coefficient.

A discrete radiation generally originates from the transition between two bound states of a particle, while the continuum radiation arises from the transition between two states in which at least one of them is a free state. Accordingly, the general form of the absorption coefficient can be written as

$$\kappa_\nu = \kappa_\nu^{\text{cont}} + \kappa_\nu^{\text{disc}}, \tag{3}$$

where κ_ν^{cont} and κ_ν^{disc} are the corresponding parts of continuum and discrete radiations in the absorption coefficient at the frequency ν.

To model the discrete emissions in the SL spectrum, the absorption coefficient for a transition between two energy levels of E_1 and E_2 for a hydrogen-like atom, with the frequency $\nu_0 = (E_1 - E_2)/h$, can be written as [16,35]

$$\kappa_\nu^{\text{disc}} = A_{21}\frac{c^2}{8\pi\nu_0^2}g(\nu,\nu_0)n_2\left(1 - e^{h\nu/k_BT_g}\right), \tag{4}$$

where A_{21} is the spontaneous Einstein coefficient for the transition and n_2 is the number density of the particles at the upper energy level E_2. Here, we only consider the discrete transitions of Xe atoms in the SL spectrum. The function $g(\nu,\nu_0)$ is the Lorentzian line profile for the transition with the central frequency ν_0

$$g(\nu,\nu_0) = \frac{\Delta\nu/2\pi}{(\nu - \nu_0)^2 + (\Delta\nu/2)^2}, \tag{5}$$

where $\Delta\nu$ is the natural broadening of the transition enlarged by the collisions of the high pressure conditions at the collapse [36]. The quantity n_2 in Eq. (4) is calculated from the partition function of Maxwell-Boltzmann distribution for the Xe atoms,

$$n_2 = n\frac{g_2e^{-E_2/k_BT}}{\sum_{E_i} g_ie^{-E_i/kT_g}}, \tag{6}$$

with n the number density of Xe atoms in the bubble and $Z = \sum_{E_i} g_ie^{-E_i/kT_g}$ is the partition function for different energies E_i and degeneracies g_i of Xe atoms. The spectroscopic data for different transitions of Xe were extracted from the NIST database [37].

The continuum part of the SL radiation occurs from the transition between free states. The transition between a bound state to a free state is known as the photoelectric absorption. However, the transition between two free states makes a bremsstrahlung emission or absorption. Since all radiation information can be extracted from the absorption coefficient, only the absorption processes should be considered

in the calculations. In the high-temperature and the high-pressure conditions of the bubble collapse, three absorption mechanisms are important:

(1) the free-free transition of electron-ion bremsstrahlung;
(2) the free-free transition of electron-atom bremsstrahlung;
(3) the bound-free transition of photoionization.

It should be mentioned that the emission processes of bremsstrahlung and recombination are the inverse phenomena of the three aforementioned absorptions and consequently they are implicitly considered in the radiation transfer equation [33]. All three absorption mechanisms strongly depend on the number density of the free electrons inside the bubble, which can be determined for a weakly ionized gas by the Saha equation:

$$\frac{n_e^2}{n-n_e} = \left(\frac{2\pi m_e k_B T}{h^2}\right)^{3/2} \exp\left[\frac{-E_{\rm ion}}{k_B T}\right], \tag{7}$$

where $E_{\rm ion}$ is the first ionization energy of Xe atoms and m_e and h are the electron mass and Planck constant, respectively. It should be mentioned that the Saha equation is valid only for a dilute plasma. Consequently, for the case of a dense plasma like an SL bubble in water, a modification of the Saha equation is required and consists of a reduction of the potential of ionization as that presented in Ref. [13]. However, in sulfuric acid, the bubble collapse seems less violent than in water and the pressure and the density reached by the bubble may be smaller. Therefore, the correction is perhaps less required. Accordingly, we restrict our calculations to the case of a dilute plasma and the normal Saha equation is used.

The absorption coefficient for the free-free transition of an electron in the Coulomb field of a positive ion Xe^+ can be written as [38]

$$\kappa_\nu^{e-i} = \frac{4}{3}\left(\frac{2\pi}{3m_e k_B T}\right)^{1/2} \frac{Z_{\rm Xe}^2 e^6}{hcm_e \nu^3} n_e^2 \tag{8}$$

where $Z_{\rm Xe}$ is the atomic number of Xe. The electron-ion bremsstrahlung absorption coefficient is proportional to the square of the electron number density.

In a weakly ionized gas, another bremsstrahlung process that should be taken into account is the electron-neutral atom bremsstrahlung. The absorption coefficient for this mechanism, which is proportional to the electron number density, can be written as [38]

$$\kappa_\nu^{e-n} = \frac{4ne^2}{3\nu^2 c}\left(\frac{2k_B T_g}{\pi m_e}\right)^{3/2}\left(3c_{\rm tr} + \frac{d_{\rm tr}}{k_B T_g}\right) n_e, \tag{9}$$

where for Xe, the parameters are $c_{\rm tr} = 1.6 \times 10^{-20}$ m^2/eV and $d_{\rm tr} = -1.39 \times 10^{-20}$ m^2 [11,39].

The third continuum absorption process is the photoionization of a neutral atom. The corresponding absorption coefficient is given by [33]

$$\kappa_\nu^{\rm ph} = \frac{64\pi^4}{3\sqrt{3}} \frac{e^{10} m_e Z_{\rm Xe}^4 n}{h^6 c \nu^3} \sum_{j=2}^{\infty} \frac{1}{j^3} \exp\left[\frac{-(E_{\rm ion} - |E_j|)}{k_B T}\right], \tag{10}$$

where, $E_j = E_{\rm ion}/j^2$. The total absorption coefficient of all continuum and discrete emissions is the sum of four mentioned absorption coefficients

$$\kappa_\nu^{\rm tot} = \kappa_\nu^{e-i} + \kappa_\nu^{e-n} + \kappa_\nu^{\rm ph} + \kappa_\nu^{\rm disc}. \tag{11}$$

The spectral SL intensity of the bubble at the collapse time can be determined from the time average of the bubble emission during the collapse given by

$$I_\nu^{\rm SL} = \frac{1}{T_l}\int_{\rm collapse} I_\nu(t)dt, \tag{12}$$

where the integration is taken on the collapse time interval, T_l. The radiated energy spectrum in the unit area is given by $I_\nu^{\rm SL} T_l$. Consequently, the radiated energy calculated in the simulation strongly depends on the value chosen for the quantity T_l. In the experiment, this quantity is determined by the response time of the photodetector used for measuring the SL radiation. In this work, we consider that T_l is of the same order as the SL time interval.

III. SIMULATION RESULTS

The simulation was carried out for three different concentrations of Xe in the concentrated solution of H_2SO_4 (85%). Figure 1 shows the phase parameters of diffusively stable SL bubbles for the Xe concentrations of 4, 20, and 50 torr. It is seen that the initial radii of the SL bubbles increases with the noble gas concentration. The radii of the 50 torr bubbles are between two and ten times greater than those of the 4 torr bubbles. Also, the driving pressures of diffusively stable bubbles are greater for lower partial pressures of Xe in the acid.

Figure 2 shows the bubble radius evolution during three periods of the ultrasound field for the concentrations of 4 and 50 torr. The driving pressures are very similar for these bubbles. The graph of "Transient" shows the radii evolutions during three first periods of the external ultrasound pressure. In this graph, we see a nonperiodic dynamic for the evolution of the bubble of 50 torr. Note that maximum radius of this bubble gradually decreases during the three periods and the bubble has a transient evolution. However, for the bubble of 4 torr, a periodic dynamic is seen during the same time interval.

The graph "Stable" shows the bubble evolutions during three periods after passing 200 initial periods of the ultrasound

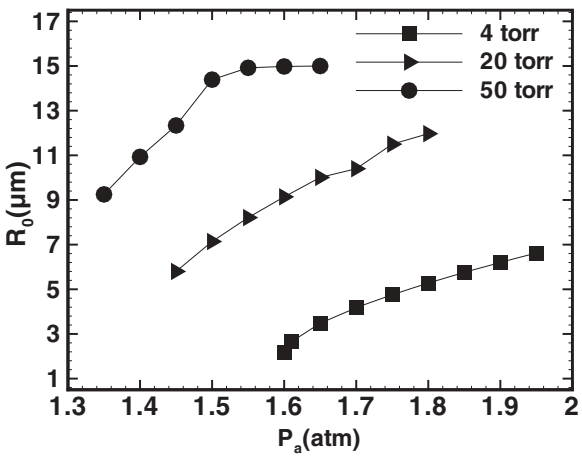

FIG. 1. The phase parameters (driving pressure P_a and initial radius R_0) for diffusively stable SL bubbles in the sulfuric acid solution (85%), containing Xe with concentrations of 4, 20, and 50 torr.

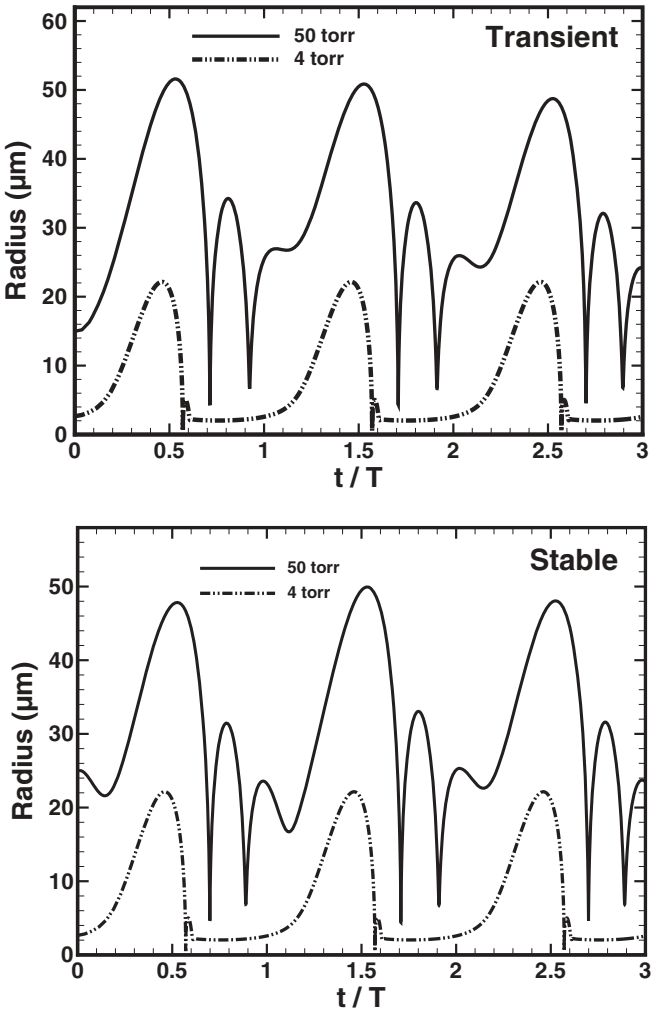

FIG. 2. The bubble radius evolution during three periods for the two concentrations of 4 and 50 torr. The driving pressures of the 4 and 50 torr bubbles are $P_a = 1.61$ atm and $P_a = 1.60$ atm, respectively. The graphs "Transient" and "Stable" show the radii evolutions at the beginning of the ultrasound field and after passing 200 periods, respectively.

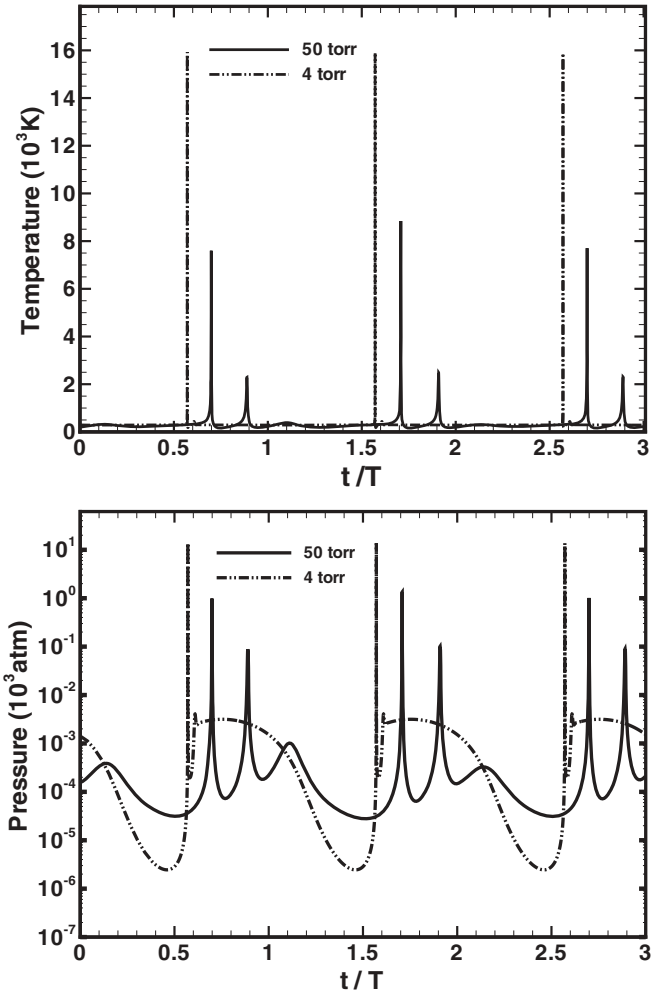

FIG. 3. The time variations of the temperatures and the pressures of the 4 and 50 torr bubbles described in the legend of Fig. 2, during the three periods of stable dynamics.

field. In this case, the dynamics of both the 4 and 50 torr bubbles are periodic. However, the periodicity of the 50 torr bubble is twice the ultrasound period. The evolution of the 50 torr bubble in this case is an example of period doubling dynamic, which has already been reported in many experiments [40–42]. So far, two different mechanisms of anisotropy for the bubble due to either the bubble translation [9,43] or breaking the spherical symmetry during the collapse [44,45] are suggested to be the origin of the period doubling phenomenon. Our results here indicate a third mechanism can be proposed for the period doubling, in which the bubble is at a fixed location and spherically oscillates. However, the long-lived rebounds after the main collapse lead to the period doubling effect. Note that no period doubling effect is seen for the 4 torr bubble. Details of our calculations show that for the high concentration of 50 torr, the radius evolution becomes completely period-doubled only after passing a large number of periods of the ultrasound field (about 100 periods).

The lack of periodicity of the 50 torr bubble in the transient evolution originates from the extension of the afterbounce oscillations from one period to the next period. This perturbs the bubble evolutions in several beginning periods resulting in the lack of periodicity in the transient curve. However, after passing a large number of periods, the 50 torr bubble adjusts its evolution with the external field in the manner that a periodic dynamic occurs. Our calculations indicate that depending on the driving pressure amplitude, the periodicity in this case can be multiple ultrasound periods (twice in Fig. 2) and this result is in agreement with experimental reports [9]. On the other hand, for the 4 torr bubble, due to the smallness of the afterbounce oscillations, the bubble reaches to its periodic evolution after the first period with the same periodicity as the external ultrasound field.

In Fig. 3, the variations of the temperatures and the pressures of the 4 and 50 torr bubbles have been shown during the stable evolution. It is seen that the peak values of the bubble temperature and pressure at the time of SL emission are considerably greater for the 4 torr bubble than the 50 torr bubble, while the driving pressures are very similar for these bubbles (1.61 atm for the 4 torr and 1.6 atm for the 50 torr).

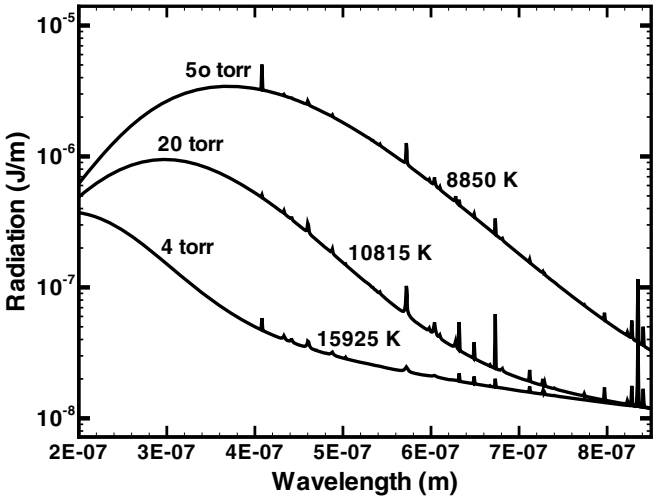

FIG. 4. Comparison of the SL spectrums of the radiated energy from the bubbles of 4, 20, and 50 torr. The 20 torr bubble is driven by the pressure of $P_a = 1.5$ atm. While the driving pressures of the 4 and 50 torr bubbles are the same as those described in the legend of Fig. 2.

The large differences between the peak pressures and the peak temperatures of these bubbles mainly originate from the large difference between the minimum radii of these bubbles (0.52 μm for the 4 torr bubble and 4.21 μm for the 50 torr bubble). The difference between the minimum radii also goes back to the difference between the initial radii of the bubbles shown in Fig. 1.

In Fig. 4, the SL spectrums of the radiated energy from the bubbles of 4 and 50 torr are shown in addition to the spectrum of a 20 torr SL bubble driven by the pressure of $P_a = 1.5$ atm. Qualitatively, the simulation results are in good agreement with the experimental results of Ref. [9] as in both cases the scale of the SL spectrum for the 50 torr bubble is between two to three orders of magnitude smaller than that of the 4 torr bubble. Further quantitative adaptation of the simulation results with experiment requires the response time of the photodetector used in the experiment for measuring the SL light emission, which is not mentioned in Ref. [9]. Although the SL temperature of the 4 torr bubble is almost twice that of the 50 torr bubble, the considerably larger light-emitting region of the 50 torr bubble leads to a remarkably greater SL emission for this bubble. This result indicates that reaching to a higher temperature is not sufficient for getting a higher SL emission from the bubble. In fact, the size of the light-emitting region is an important factor, which may show that a hotter SL bubble has a lower SL radiation.

The coherency of the results of Fig. 4 with the experimental results of Ref. [9] seems to propose a way for resolving the problem of incompatibility between the temperatures of the line and the continuum emissions in experiment. Since the results of the simulation are obtained with a common temperature for both discrete and continuum emissions, this suggests that the experimental incompatibility can possibly be removed by fitting the experimental spectrum with a proper model of SL, including simultaneous effects of both line and continuum emissions. In the experimental works, the continuum spectrum is fitted by the black body or simple bremsstrahlung spectrum. The incompleteness of the modeling may produce an error in the temperature obtained from the fitting and this error can be removed by a proper model for the SL spectrum.

To provide a more complete insight about dependency of SL intensity on the temperature and the size of the light-emitting region, the results of variations of the temperature, the intensity, and the minimum radius with variation of driving pressure are shown in Fig. 5. It is seen that the range of SL temperature of the 50 torr bubble is between 4000 and 9000 K. While the temperature of the 4 torr bubble increases from 9000 K to more than 40000 K. Note that for most driving pressures, both the temperature and the SL intensity of the 4 torr bubble are considerably greater than those of the 50 torr bubble. However, the minimum radius of the 4 torr bubble is between six and ten times smaller than the 50 torr bubble.

In Fig. 5, we also see that around the driving pressure of $P_a = 1.6$ atm, the SL intensity of the 4 torr bubble can be about three orders of magnitude smaller than the 50 torr bubble. Similar to this result was that observed in the experiment of Ref. [9]. In this case, the light-emitting region of the 50 torr bubble is more than 500 times greater than the 4 torr bubble. The results of this figure indicate that although both the temperature and the size of the light-emitting region are important for determination of the SL intensity, the temperature has a more significant role on the SL intensity. This mainly arises from the exponential dependency of the SL intensity on the bubble temperature against the direct proportionality of the intensity to the bubble volume.

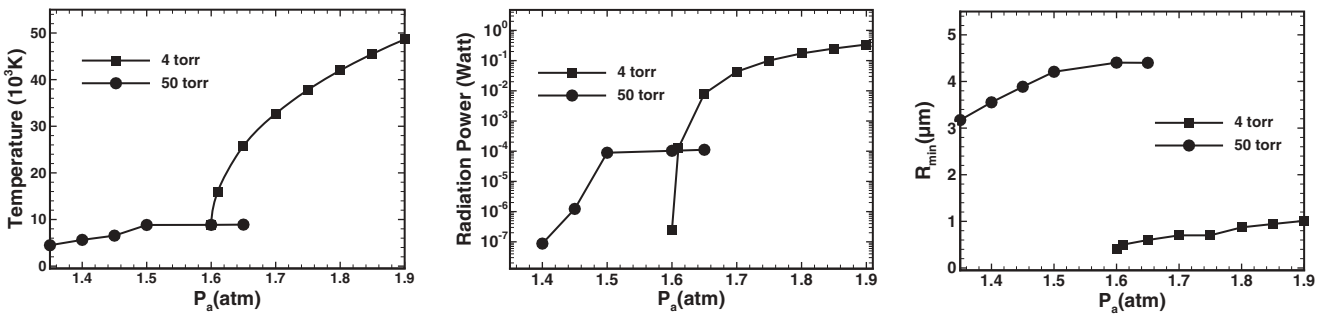

FIG. 5. Variations of the SL temperature, the SL radiated power, and the minimum radius for Xe bubbles of 4 and 50 torr with variation of the driving pressure.

IV. CONCLUSIONS

In this work using a radiation model including effects of both continuum and line emissions, the spectral intensity of an Xe sonoluminescing bubble was simulated. Considering various driving pressures for the bubbles of 4 and 50 torr, it was shown that in agreement with the experiment, the periodicity of the bubble dynamics for a 50 torr bubble can be multiple ultrasound periods. While for a 4 torr bubble, the same periodicity as the ultrasound period is observed. Also, the temperature and the intensity of SL for most of allowable driving pressures of the 4 torr bubble are greater than those of the 50 torr bubble. However, for the range of driving pressures that the 50 torr bubble is near its maximum driving conditions, its SL spectral emission can be up to three orders of magnitude greater than the SL emission of the 4 torr bubble. The latter result is also in agreement with experimental reports. The simulation suggests that the intriguing experimental result of two different temperatures for the line and the continuum emissions can possibly be resolved by fitting the data with a more complete model of SL, including simultaneous effects of both line and continuum emissions.

ACKNOWLEDGMENT

This work has been supported by Tarbiat Modares University (TMU).

[1] D. F. Gaitan *et al.*, J. Acoust. Soc. Am. **91**, 3166 (1992).
[2] B. Barber *et al.*, Phys. Rep. **281**, 65 (1997).
[3] R. Hiller, S. J. Putterman, and B. P. Barber, Phys. Rev. Lett. **69**, 1182 (1992).
[4] J. B. Young, J. A. Nelson, and W. Kang, Phys. Rev. Lett. **86**, 2673 (2001).
[5] A. Troia, D. Madonna Ripa, and R. Spagnolo, Ultrasonics Sonochem. **13**, 278 (2006).
[6] D. J. Flannigan and S. K. Suslick, Acoust. Res. Lett. Online **6**, 157 (2005).
[7] D. J. Flannigan and K. S. Suslick, Phys. Rev. Lett. **95**, 044301 (2005).
[8] D. J. Flannigan and S. K. Suslick, Nature (London) **434**, 52 (2005).
[9] S. D. Hopkins, S. J. Putterman, B. A. Kappus, K. S. Suslick, and C. G. Camara, Phys. Rev. Lett. **95**, 254301 (2005).
[10] S. Hilgenfeldt, S. Grossmann, and D. Lohse, Nature (London) **398**, 402 (1999).
[11] S. Hilgenfeldt, S. Grossmann, and D. Lohse, Phys. Fluids **11**, 1318 (1999).
[12] N. Xu, L. Wang, and X. Hu, Phys. Rev. E **61**, 2611 (2000).
[13] D. Hammer and L. Frommhold, Phys. Rev. E **65**, 046309 (2002).
[14] C. Ying, Y. An, and C. Xie, J. Phys. D: Appl. Phys. **38**, 2489 (2005).
[15] Y. An, Chinese Phys. B **17**, 2984 (2008).
[16] Y. An and C. Li, Phys. Rev. E **78**, 046313 (2008).
[17] Y. An and C. Li, Phys. Rev. E **80**, 046320 (2009).
[18] Y. An and W. Zhang, Chinese Phys. B **21**, 017806 (2012).
[19] G. Vazquez, C. Camara, S. Putterman, and K. Weninger, Opt. Lett. **26**, 575 (2001).
[20] G. Vazquez, C. Camara, S. J. Putterman, and K. Weninger, Phys. Rev. Lett. **88**, 197402 (2002).
[21] K. Yasui, Phys. Rev. E **56**, 6750 (1997).
[22] B. D. Storey and A. J. Szeri, Proc. R. Soc. London A **457**, 1685 (2001).
[23] R. Toegel, S. Hilgenfeldt, and D. Lohse, Phys. Rev. Lett. **88**, 034301 (2002).
[24] A. Moshaii *et al.*, Phys. Lett. A **372**, 1283 (2008).
[25] R. Toegel and D. Lohse, J. Chem. Phys. **118**, 1863 (2003).
[26] A. Moshaii, Kh. Imani, and M. Silatani, Phys. Rev. E **80**, 046325 (2009).
[27] A. Moshaii and R. Sadighi-Bonabi, Phys. Rev. E **70**, 016304 (2004).
[28] A. Moshaii, S. Tajik-Nezhad, and M. Faraji, Phys. Rev. E **84**, 046301 (2011).
[29] A. Moshaii, M. Faraji, and S. Tajik-Nezhad, Ultrasonics Sonochem. **18**, 1148 (2011).
[30] W. C. Moss, D. A. Young, J. A. Harte, J. L. Levatin, B. F. Rozsnyai, G. B. Zimmerman, and I. H. Zimmerman, Phys. Rev. E **59**, 2986 (1999).
[31] B. D. Storey and A. J. Szeri, Proc. R. Soc. London A **456**, 1685 (2000).
[32] Y. An, Phys. Rev. E **74**, 026304 (2006).
[33] Ya. B. Zeldovich and Yu. P. Raizer, *Physics of Shock Waves and High-Temperature Hydrodynamics Phenomena* (Academic Press, New York, 1996).
[34] G. B. Arfken and H. J. Weber, in *Mathematical Methods for Physicists*, 5th ed. (Academic Press, San Diego, 2001), p. 501.
[35] G. B. Rybicki *et al.*, in *Radiative Processes in Astrophysics* (Wiley-VCH, Weinheim, 2004), pp. 27–33.
[36] K. R. Lang, in *A Compendium for the Physicist and Astrophysicist* (Springer, Berlin, 1974), p. 211.
[37] NIST, *Chemistry Webbook* (2005), http://webbook.nist.gov/chemistry/.
[38] D. Hammer and L. Frommhold, Journal of Modern Optics **48**, 239 (2001).
[39] L. Frommhold, Phys. Rev. E **58**, 1899 (1998).
[40] R. G. Holt, D. F. Gaitan, A. A. Atchley, and J. Holzfuss, Phys. Rev. Lett. **72**, 1376 (1994).
[41] M. T. Levinsen, N. Weppenaar, J. S. Dam, G. Simon, and M. Skogstad, Phys. Rev. E **68**, 035303 (2003).
[42] J. S. Dam, M. T. Levinsen, and M. Skogstad, Phys. Rev. Lett. **89**, 084303 (2002).
[43] J. S. Dam and M. T. Levinsen, Phys. Rev. Lett. **94**, 174301 (2005).
[44] Y. An, T. Lu, and B. Yang, Phys. Rev. E **71**, 026310 (2005).
[45] J. Holzfuss, Phys. Rev. E **77**, 066309 (2008).